

RESEARCH ARTICLE

# Quantitative *in vivo* mapping of myocardial mitochondrial membrane potential

Nathaniel M. Alpert<sup>1\*</sup>, Nicolas Guehl<sup>1</sup>, Leon Ptaszek<sup>2</sup>, Matthieu Pelletier-Galarneau<sup>1</sup>, Jeremy Ruskin<sup>2</sup>, Moussa C. Mansour<sup>2</sup>, Dustin Wooten<sup>1</sup>, Chao Ma<sup>1</sup>, Kazue Takahashi<sup>1</sup>, Yun Zhou<sup>3</sup>, Timothy M. Shoup<sup>1</sup>, Marc D. Normandin<sup>1</sup>, Georges El Fakhri<sup>1</sup>

**1** Gordon Center for Medical Imaging, Massachusetts General Hospital, Harvard Medical School, Boston, Massachusetts, United States of America, **2** Cardiac Arrhythmia Service, Massachusetts General Hospital, Harvard Medical School, Boston, Massachusetts, United States of America, **3** The Russell H. Morgan Department of Radiology and Radiological Science, School of Medicine Johns Hopkins University, Baltimore, Maryland, United States of America

\* [alpert@pet.mgh.harvard.edu](mailto:alpert@pet.mgh.harvard.edu)



## Abstract

### Background

Mitochondrial membrane potential ( $\Delta\Psi_m$ ) arises from normal function of the electron transport chain. Maintenance of  $\Delta\Psi_m$  within a narrow range is essential for mitochondrial function. Methods for *in vivo* measurement of  $\Delta\Psi_m$  do not exist. We use <sup>18</sup>F-labeled tetraphenylphosphonium (<sup>18</sup>F-TPP<sup>+</sup>) to measure and map the total membrane potential,  $\Delta\Psi_T$ , as the sum of  $\Delta\Psi_m$  and cellular ( $\Delta\Psi_c$ ) electrical potentials.

### Methods

Eight pigs, five controls and three with a scar-like injury, were studied. Pigs were studied with a dynamic PET scanning protocol to measure <sup>18</sup>F-TPP<sup>+</sup> volume of distribution,  $V_T$ . Fractional extracellular space ( $f_{ECS}$ ) was measured in 3 pigs. We derived equations expressing  $\Delta\Psi_T$  as a function of  $V_T$  and the volume-fractions of mitochondria and  $f_{ECS}$ . Seventeen segment polar maps and parametric images of  $\Delta\Psi_T$  were calculated in millivolts (mV).

### Results

In controls, mean segmental  $\Delta\Psi_T = -129.4 \pm 1.4$  mV (SEM). In pigs with segmental tissue injury,  $\Delta\Psi_T$  was clearly separated from control segments but variable, in the range -100 to 0 mV. The quality of  $\Delta\Psi_T$  maps was excellent, with low noise and good resolution. Measurements of  $\Delta\Psi_T$  in the left ventricle of pigs agree with previous *in-vitro* measurements.

### Conclusions

We have analyzed the factors affecting the uptake of voltage sensing tracers and developed a minimally invasive method for mapping  $\Delta\Psi_T$  in left ventricular myocardium of pigs.  $\Delta\Psi_T$  is computed in absolute units, allowing for visual and statistical comparison of individual values

## OPEN ACCESS

**Citation:** Alpert NM, Guehl N, Ptaszek L, Pelletier-Galarneau M, Ruskin J, Mansour MC, et al. (2018) Quantitative *in vivo* mapping of myocardial mitochondrial membrane potential. PLoS ONE 13 (1): e0190968. <https://doi.org/10.1371/journal.pone.0190968>

**Editor:** Cecilia Zazueta, Instituto Nacional de Cardiologia Ignacio Chavez, MEXICO

**Received:** October 20, 2017

**Accepted:** December 22, 2017

**Published:** January 16, 2018

**Copyright:** © 2018 Alpert et al. This is an open access article distributed under the terms of the [Creative Commons Attribution License](https://creativecommons.org/licenses/by/4.0/), which permits unrestricted use, distribution, and reproduction in any medium, provided the original author and source are credited.

**Data Availability Statement:** All relevant data are available at: doi:[10.7910/DVN/07YOKO](https://doi.org/10.7910/DVN/07YOKO).

**Funding:** This work was funded by two grants from the United States National Institutes of Health: R01HL110241 (GEF) and R01HL137230 (GEF), <https://www.nih.gov>. These grants were awarded as part of the standard peer review process for new grants. The study design and analysis are solely the work of the study authors, meaning that the funders had no role in study

design, data collection and analysis, decision to publish, or preparation of the manuscript.

**Competing interests:** The authors have declared that no competing interests exist.

with normative data. These studies demonstrate the first in vivo application of quantitative mapping of total tissue membrane potential,  $\Delta\Psi_T$ .

## Introduction

Mitochondria produce approximately 90% of cellular adenosine triphosphate (ATP) through oxidative phosphorylation [1]. The electron transport chain (ETC) of the mitochondrion is ultimately responsible for converting the foods we eat into electrical and chemical energy gradients by pumping protons across the inner membrane in the mitochondrial intermembrane space. The energy stored in the electric field, referred to as mitochondrial membrane potential ( $\Delta\Psi_m$ ), is then used to power the conversion of ADP to ATP. In a typical cell, the  $\Delta\Psi_m$  remains constant with time and is about -140 mV [2]. Table 1 lists  $\Delta\Psi_m$  for mitochondria of different cell types.

If  $\Delta\Psi_m$  remains within the physiological range, a small amount of reactive oxygen species (ROS) is produced. However, in mitochondrial dysfunction,  $\Delta\Psi_m$  falls outside the normal range, with concomitant increase in ROS release, and impairment of ATP production [10]. And because mitochondria are the most important source of energy and ROS in the cell, mitochondrial dysfunction is at the core of many diseases, including myopathies [11], diabetes [12], degenerative diseases [13], inflammation [14], cancer [15], and cardiac arrhythmias [16, 17].

Despite continuing scientific interest in voltage sensitive probes, a noninvasive method for measuring  $\Delta\Psi_m$  in living animals does not currently exist. The basic physiological studies conducted several decades ago are highly relevant but not always mentioned: Historically, fluorescent dyes [18] and lipophilic cationic tracers have been developed for quantitative assay of  $\Delta\Psi_m$  in isolated mitochondria [4], cells [19], and isolated heart preparations [6]. Electrodes sensitive to tetraphenylphosphonium (TPP) have also been developed and used to evaluate  $\Delta\Psi_m$  in isolated mitochondrial fractions [9, 20]. [<sup>14</sup>C or <sup>3</sup>H]-labeled lipophilic cations were used to study the electrical properties of membranes and mitochondria long before modern imaging methods were imagined [3, 21–23]. More recently, Logan et al. [24] reported a "click" method for in vivo measurement of  $\Delta\Psi$  in the cells of mouse hearts, but their method requires the excision of the heart and hence is not suitable for translation to human studies.

The work cited above established the use of <sup>3</sup>H-TPP<sup>+</sup> as a reference tracer for measuring mitochondrial membrane potential ( $\Delta\Psi_m$ ). Investigators have shown that <sup>3</sup>H-TPP<sup>+</sup> distributes

**Table 1. Measured values of mitochondrial membrane potential (millivolts).**

Authors	Preparation	Tracer Method	$\Delta\Psi_m$ (mV)	$\Delta\Psi_T$ (mV)
This work	in vivo swine heart	<sup>18</sup> F-TPP <sup>+</sup> PET	_____	-129
Kaappinen, R.[3]	perfused rat hearts	<sup>3</sup> H-TPMP <sup>+</sup>	-125	
Rottenburg, H.[4]	rat liver	<sup>3</sup> H-TPP <sup>+</sup>	-150	
LaNoue, et al.[5]	isolated brown adipocytes	<sup>3</sup> H-TPP <sup>+</sup>	-116	
Wan, et al.[6]	perfused rat hearts	<sup>3</sup> H-TPP <sup>+</sup>	-145	
Gurm, et al.[7]	in vivo swine heart	<sup>18</sup> F-TPP <sup>+</sup>	-91	
Gerencser et al. [8]	cultured neurons (resting)	Fluorescent probe	-139	
Kamo et al.[9]	isolated mitochondria (state 4)	TPP <sup>+</sup> electrode	-180	

Column 1 indicates the author(s) of each study. Column 2 indicates the conditions of measurement, e.g. isolated cells. Column 3 indicates the methodology used in the measurement. Column 4 list the value of  $\Delta\Psi_m$ . Column 5 lists the value of  $\Delta\Psi_T$

<https://doi.org/10.1371/journal.pone.0190968.t001>

slowly in accord with the electrochemical gradient [4, 22]. Min et al suggested that TPP might be an important imaging agent [25]. By replacing the tritium label with  $^{18}\text{F}$  [26], it is possible to adapt the methodology to PET, making it feasible to extend these measurements to intact animals and to human studies. In this paper, we report work that adapts the methods used in the earlier bench top measurements to in vivo imaging using positron emission tomography (PET/CT) to measure and map total membrane potential ( $\Delta\Psi_T$ ). We define  $\Delta\Psi_T$  as the sum of  $\Delta\Psi_m$  and cellular ( $\Delta\Psi_c$ ) electrical potentials. The time scale of our measurements are tens of minutes and thus  $\Delta\Psi_c$  is represented by its time average.  $\Delta\Psi_T$  is chosen as a practical surrogate for  $\Delta\Psi_m$ , keeping in mind that in most situations  $\Delta\Psi_m \approx 10^* \Delta\Psi_c$  and thus  $\Delta\Psi_T \approx \Delta\Psi_m$ . In our methodology a cationic lipophilic tracer TPP<sup>+</sup>, labeled with  $^{18}\text{F}$ , is used to quantitatively map myocardial  $\Delta\Psi_T$ .  $^{18}\text{F}$ -TPP<sup>+</sup> was initially developed as a myocardial flow imaging agent under the trade name BFPET [26]. However,  $^{18}\text{F}$ -TPP<sup>+</sup> enters the tissue with a low first-pass extraction fraction and does not respond to pharmacological challenge with a stressor and hence cannot be considered a flow tracer [7]. Nonetheless, its electrochemical properties make it a tracer of interest for quantitative imaging of  $\Delta\Psi_T$ .

Previous work, attempting to detect changes in concentration due to alteration of the  $\Delta\Psi_m$  used tracers such as  $^{99\text{m}}\text{Tc}$ -sestamibi [27], tetraphenyl phosphonium [25], (18F-fluoropentyl) triphenylphosphonium [28], and  $^{18}\text{F}$ -fluorobenzyl triphenyl phosphonium [29] [30], with semi-quantitative endpoints such as SUV [31]. The results of these studies are empirical and descriptive. In the sense that a binary decision threshold is sought; the electrical properties of transmembrane kinetics are not exploited for quantitative purposes. Changes indicative of graded mitochondrial dysfunction cannot be detected. Gurm et al reported the first attempt to quantitatively measure  $\Delta\Psi_m$  with PET and  $^{18}\text{F}$ -TPP<sup>+</sup> [7]. Their analysis simply applied the Nernst equation to the PET and plasma concentrations measured 30 minutes after bolus injection of  $^{18}\text{F}$ -TPP<sup>+</sup>. But terminating the study at 30 minutes was arbitrary and did not consider that the plasma level falls monotonically for at least 120 minutes, meaning that had they used the data at, say, 45 minutes after injection, they would have obtained a different result. Thus, their assumption that tracer was in steady state 30 minutes after bolus injection is incorrect and leads to biased results. In addition, their analysis did not consider the effect of tracer in the extracellular space. Because of these errors, their method violates basic tracer kinetic principles and their results significantly underestimate  $\Delta\Psi_m$  and are not in good agreement with work from in vitro studies (Table 1).

## General design of the studies

This investigation provides an initial assessment of a method for quantitative mapping of  $\Delta\Psi_T$ . Because the mammalian heart has the highest concentration of mitochondria, we chose myocardial imaging as the first application to facilitate optimization of the scanning conditions. The subjects of our study were domestic swine (*Sus domesticus*) imaged in one of two conditions: healthy controls or pigs with chronic injury to the left anterior descending arterial (LAD) territory. We used bolus injection of  $^{18}\text{F}$ -TPP<sup>+</sup> in control and injured pigs to measure the kinetics of TPP<sup>+</sup> for at least two hours, determining the volume of distribution by a regression model.

## Methods

### A new method for quantification of membrane potential

We partition the tissue distribution of  $^{18}\text{F}$ -TPP<sup>+</sup> into several components: ECS, consisting of interstitial space and plasma, mitochondria (mito) and cytosolic (cyto) volume fractions (Fig 1). The Nernst equation [32, 33] equates transmembrane electric potential to the ratio of ion concentrations on either side of the membrane. Thus, the Nernst equation allows us to derive

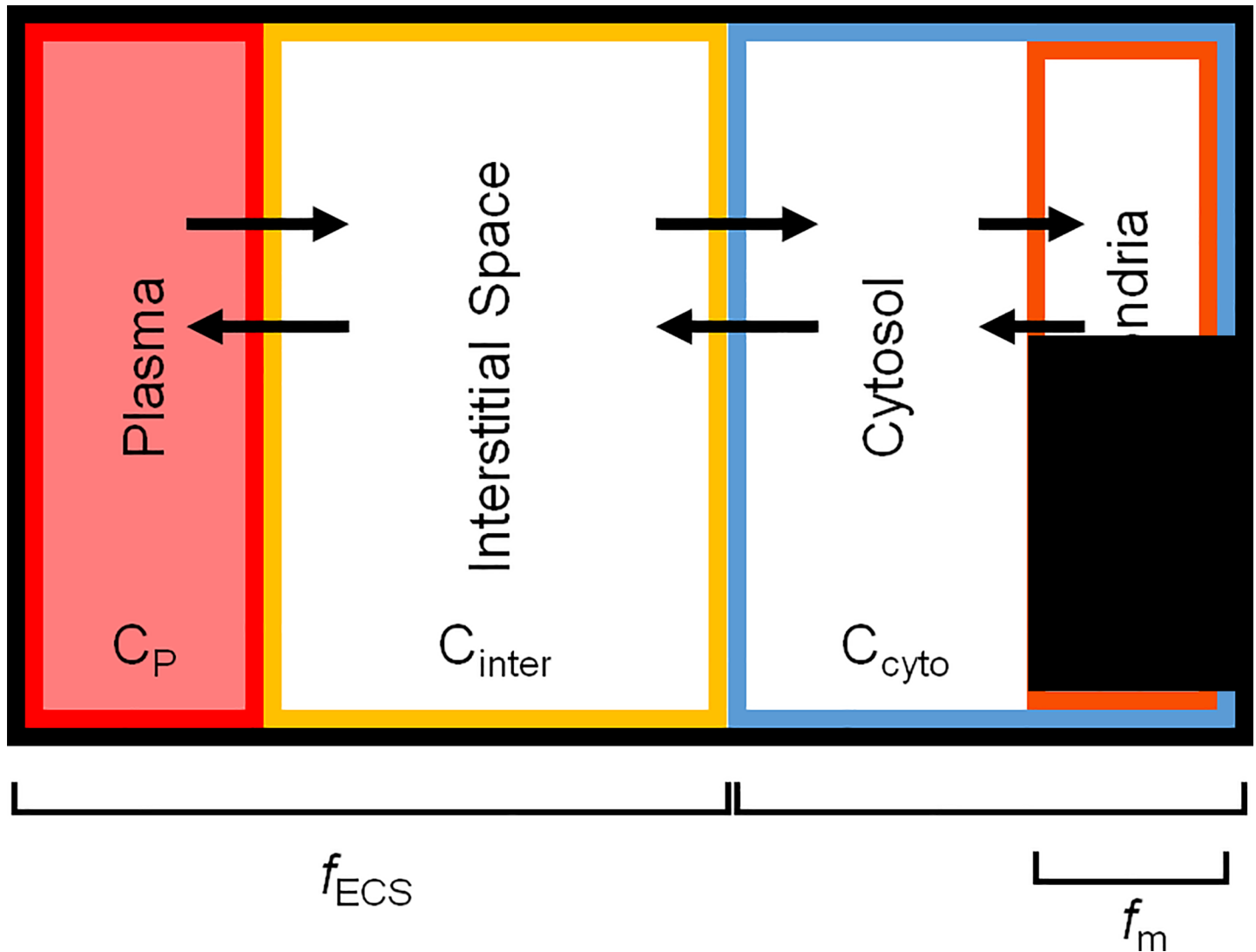


**Fig 1. Volume of distribution model for  $^{18}\text{F-TPP}^+$  in a PET image voxel.** The outer black line represents the voxel boundary.  $C_P$ ,  $C_{\text{inter}}$ ,  $C_{\text{cyto}}$ , and  $C_{\text{mito}}$  represent the concentrations of the plasma, interstitial space, cytosol, and mitochondria respectively. The arrows represent  $^{18}\text{F-TPP}^+$  transport between the different compartments.  $f_{\text{ECS}}$  represents the voxel volume fraction occupied by ECS and  $f_{\text{mito}}$  represents the cellular volume fraction occupied by mitochondria.

<https://doi.org/10.1371/journal.pone.0190968.g001>

an equation relating the PET measurements of  $^{18}\text{F-TPP}^+$  concentration, to  $\Delta\Psi_T$ , ECS fraction ( $f_{\text{ECS}}$ ), mitochondrial volume fraction ( $f_{\text{mito}}$ ) and the electric potential across the cellular membrane,  $\Delta\Psi_c$ . At steady state, the concentration of  $^{18}\text{F-TPP}^+$  in a PET voxel can be written as

$$\bar{C}_{\text{PET}} = (1 - f_{\text{ECS}})(f_{\text{mito}} \cdot \bar{C}_{\text{mito}} + (1 - f_{\text{mito}}) \cdot \bar{C}_{\text{cyto}}) + f_{\text{ECS}} \cdot \bar{C}_{\text{ECS}} \quad (1)$$

where,  $\bar{C}_{\text{mito}}$ ,  $\bar{C}_{\text{cyto}}$  and  $\bar{C}_{\text{ECS}}$  are the steady state concentrations of  $\text{TPP}^+$  in the mitochondria, cytosol and ECS, respectively. At steady state plasma and ECS are equal and  $\bar{C}_{\text{mito}}$  and  $\bar{C}_{\text{cyto}}$  are related through the Nernst equations:

$$\frac{\bar{C}_{\text{cyto}}}{\bar{C}_{\text{ECS}}} = e^{-\beta\Delta\Psi_c} \quad \text{and} \quad \frac{\bar{C}_{\text{mito}}}{\bar{C}_{\text{cyto}}} = e^{-\beta\Delta\Psi_m} \quad (2)$$

We divide Eq 1 by  $\bar{C}_p$  and use Eq 2 to express the tracer volume of distribution,  $V_T$ , as

$$V_T = \frac{\bar{C}_{PET}}{\bar{C}_p} = (1 - f_{ECS})(f_{mito} \cdot e^{-\beta\Delta\Psi_T} + (1 - f_{mito}) \cdot e^{-\beta\Delta\Psi_c}) + f_{ECS}, \quad (3)$$

where  $\beta = \frac{zF}{RT}$  is a ratio of known physical parameters: F denotes Faraday's constant, z is the valence, R is the universal gas constant and T is the temperature in degrees Kelvin. In our calculations  $z = 1$ ,  $F = 96485.3$  [Coulombs per mole],  $R = 8.314472$ , and  $T = 310.2$  [degrees Kelvin].  $\frac{\bar{C}_{PET}}{\bar{C}_p}$  is the steady-state ratio of the tissue to plasma concentrations. This equation predicts that  $V_T$ , a kinetically determined tracer quantity, is equal to the steady state concentration ratio  $\frac{\bar{C}_T}{\bar{C}_p}$ . Thus, when the tracer concentrations in tissue and plasma are time-invariant,  $V_T$  is, by definition, the tissue-to-plasma concentration ratio; whereas, after bolus injection the tissue-to-plasma concentration ratio varies with time and  $V_T$  must be determined kinetically.

Unlike tracers whose distribution is governed by passive transport,  $^{18}\text{F-TPP}^+$  will have a very high ( $\gg 1$ ) volume of distribution when the membrane potential is in the normal range. A reasonable approximation to the volume of distribution is given by

$$V_T = \frac{\bar{C}_T}{\bar{C}_p} \approx (1 - f_{ECS}) \cdot f_{mito} \cdot e^{-\beta\Delta\Psi_T} \quad (4)$$

Barth et al. [34] have studied 10 different mammalian species, including pigs and man, finding that the myocardial  $f_{mito}$  is a specific and constant value for any particular species. Therefore,  $V_T$  is sensitive to two independent variables;  $\Delta\Psi_T$  and  $f_{ECS}$ . The fundamental mathematical relationships expressed in Eqs 1, 2 and 3 are depicted in Fig 2, illustrating that the systematic error in  $\Delta\Psi_T$  due to neglecting  $f_{ECS}$  for normal values of  $V_T$  is about 20 mV. But note that Fig 2 also shows that at low membrane potential, the effect of the ECS is negligible, meaning that knowledge of  $f_{ECS}$  is most important for detecting normal versus mildly dysfunctional mitochondria.

## Study cohort

$^{18}\text{F-TPP}^+$  scans were performed on eight Yorkshire swine (Pigs were all American Yorkshire male ordered from Animal Bioware™ Series II Software Suite, vendor: Tufts). There were 5 animals without tissue injury, referred to as control pigs, and 3 animals with a left anterior descending artery (LAD) infarction, referred to as injury pigs. Pigs shared a room with other animals of the same species, individually housed in their own cage, free to turn and make normal movements and postural adjustments. The animals were given play toys to enrich their environment and fed adequately, with ready access to water, to ensure normal growth. An acclimation period greater than 4 days was observed upon the animal's arrival before conducting the first imaging procedure.

Animals used in this study were housed and maintained under the supervision of the Massachusetts General Hospital Animal Care and Use Committee and our study was conducted under a protocol approved by the Institutional Animal Care and Use Committee of the Massachusetts General Hospital.

## Anesthesia

Following a 12 hour fast, pigs were sedated with 4.4 mg/kg Telazol. Anesthesia was induced with isoflurane 5% and maintained with 1.5% isoflurane. During anesthesia, the animals were

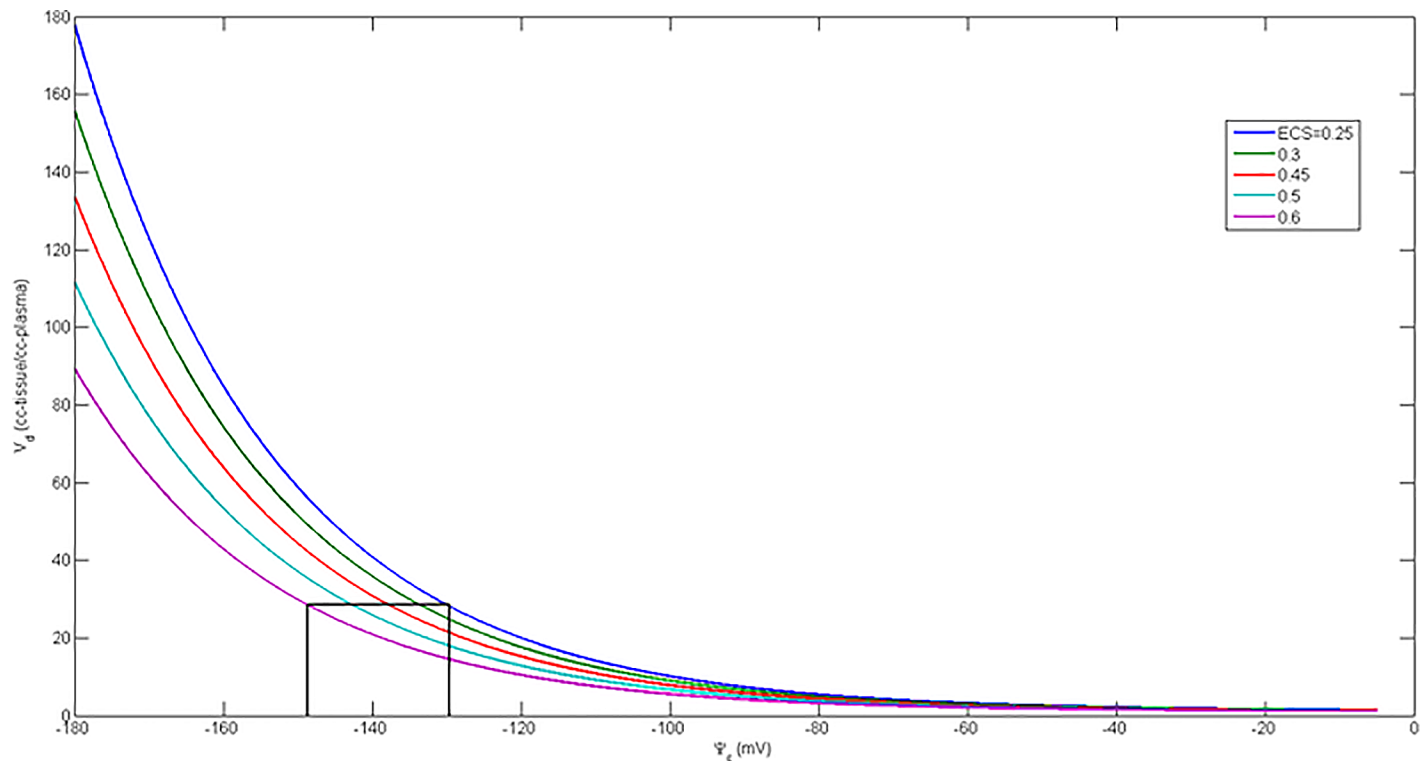


**Fig 2. Dependence of  $V_d$  on mitochondrial membrane potential and fractional ECS computed with Eq 3.**  $\Delta T$  is more negative inside membranes. Black lines indicate variation (systematic error) in  $\Delta T$  range at constant volume of distribution due to neglecting fractional ECS volume.

<https://doi.org/10.1371/journal.pone.0190968.g002>

mechanically ventilated. Vital signs and depth of anesthesia were assessed once every 5 minutes and this assessment was documented every 15 minutes.

### Tissue injury

Percutaneous central access was achieved via the Seldinger technique [35] under anesthesia. Femoral artery access was obtained and a guide wire was advanced into the LAD coronary artery. A balloon catheter was fed over the guidewire, placed in the mid LAD, and inflated to 6–8 atm for 80 minutes. An infarct was confirmed by the appearance of large ST elevation on ECG. At the end of the surgical procedure, subcutaneous Carprofen was administered and the animal was returned to housing for recuperation. After the immediate postoperative period, the animals were observed at least twice daily by study staff. Post-procedural Carprofen was administered orally for 3 days at a dose of 150 mg/day and then as needed if stiffness or swelling continued after that point. In order to prevent arrhythmias, 200mg Amiodarone and 50 mg Atenolol were also given orally every day during 2 weeks.

During the study, animal health and well-being, as well as the adequacy of anesthesia, were monitored by checking respiration rate, ECG, blood gas, corneal or palpebral reflex, blood pressure, heart rate, pulse oximetry.

### Blood sampling

Radiotracer injection, iodinated contrast injection, gadolinium injection, and venous blood sampling were performed through femoral vein catheters. An arteriovenous shunt was placed in the left femoral artery for arterial blood sampling. After tracer injection, arterial blood

samples were obtained every 10 seconds for the first 3 minutes, then at 1 minute intervals for 5 minutes, and at increasing intervals until 120 minutes post injection. Venous blood samples were obtained at 5, 10, 15, 30, 60 and 90 minutes after tracer injection. All blood samples were centrifuged to determine plasma and red cell concentration histories.

## Scanning

Eight scans, 5 control and 3 injury pigs, were performed using a Siemens Biograph 64 PET/CT. Following administration of 185 MBq of  $^{18}\text{F}$ -TPP<sup>+</sup> as a single intravenous bolus, scanning was performed over 120 minutes in list mode. CT angiography was performed for anatomic reference. List mode data were framed as a dynamic series of 12x3, 9x5, 7x10, 15x30 second frames. PET/CT data were reconstructed using a filtered back projection algorithm with CT-based attenuation correction to yield a radioactivity concentration map in units of Bq/cc with 83 slices and a voxel size of 2.14x2.14x3 mm<sup>3</sup>.  $f_{\text{ECS}}$  was measured in 3 injury pigs with CT scanning using a bolus plus infusion iodinated contrast protocol [36].

## Data analysis

Dynamic PET data were analyzed using a Logan regression method [37] to produce quantitative parametric images of the  $V_T$  of  $^{18}\text{F}$ -TPP<sup>+</sup>. Images of  $V_T$  were reoriented into the short axis projection and cropped so that the cardiac chambers occupied nearly all of the image space. Eq 3 was used to convert the parametric maps of  $V_T$  to maps of  $\Delta\Psi_T$ , assuming  $\Delta\Psi_c = -15$  mV [7] and  $f_{\text{mito}} = 0.26$  [34]. Segmental values are reported as a grand mean  $\Delta\Psi_T$  and its standard error of the mean (SEM). No background subtraction or thresholding was applied to the parametric images of  $V_T$ .

## Results

### In vivo mapping of $\Delta\Psi_T$

Fig 2 was computed using Eq 3 to show the predicted behavior of mitochondrial membrane potential as a function of total volume of distribution, and size of the extracellular space.  $\Delta\Psi_c$  was assumed to be -15 mV for these calculations. Fig 2 shows a nearly exponential behavior and that  $\Delta\Psi_T$  is nearly independent of  $f_{\text{ECS}}$  when membrane potential drops below about -100 mV.

As shown in Fig 3, after bolus injection, the plasma concentration history decreased rapidly during the "equilibration" phase and slowly thereafter; whereas, TPP demonstrated an extended myocardial residence time characterized by nearly constant or slowly decreasing tissue concentration. The concentration ratio for whole blood versus plasma became constant, with a mean value of  $0.98 \pm 0.02$  (SEM), about 15 minutes after injection of TPP<sup>+</sup> (Fig 4). Venous and arterial samples obtained later than 10 minutes after injection of TPP<sup>+</sup> were in good agreement.

$^{18}\text{F}$ -TPP<sup>+</sup> concentration was highest in heart and liver, reaching a plateau in normal myocardium after about 10 minutes and declining very slowly thereafter. The uptake of  $^{18}\text{F}$ -TPP<sup>+</sup> in scar was variable, reflecting the variation in degree and extent of injury. Tissue concentration in the injured area peaked about 10 minutes after injection, followed by a slow biphasic clearance, with the plateau level about 40% as high as in the normal myocardium. In normal left ventricular myocardium, average  $f_{\text{ECS}} = 0.20$  and varied less than 10%. Local values of  $f_{\text{ECS}}$  could not be obtained in the tissue injury, due to poor signal-to-noise ratio in the CT-studies and average values were used in computation of  $\Delta\Psi_T$ .

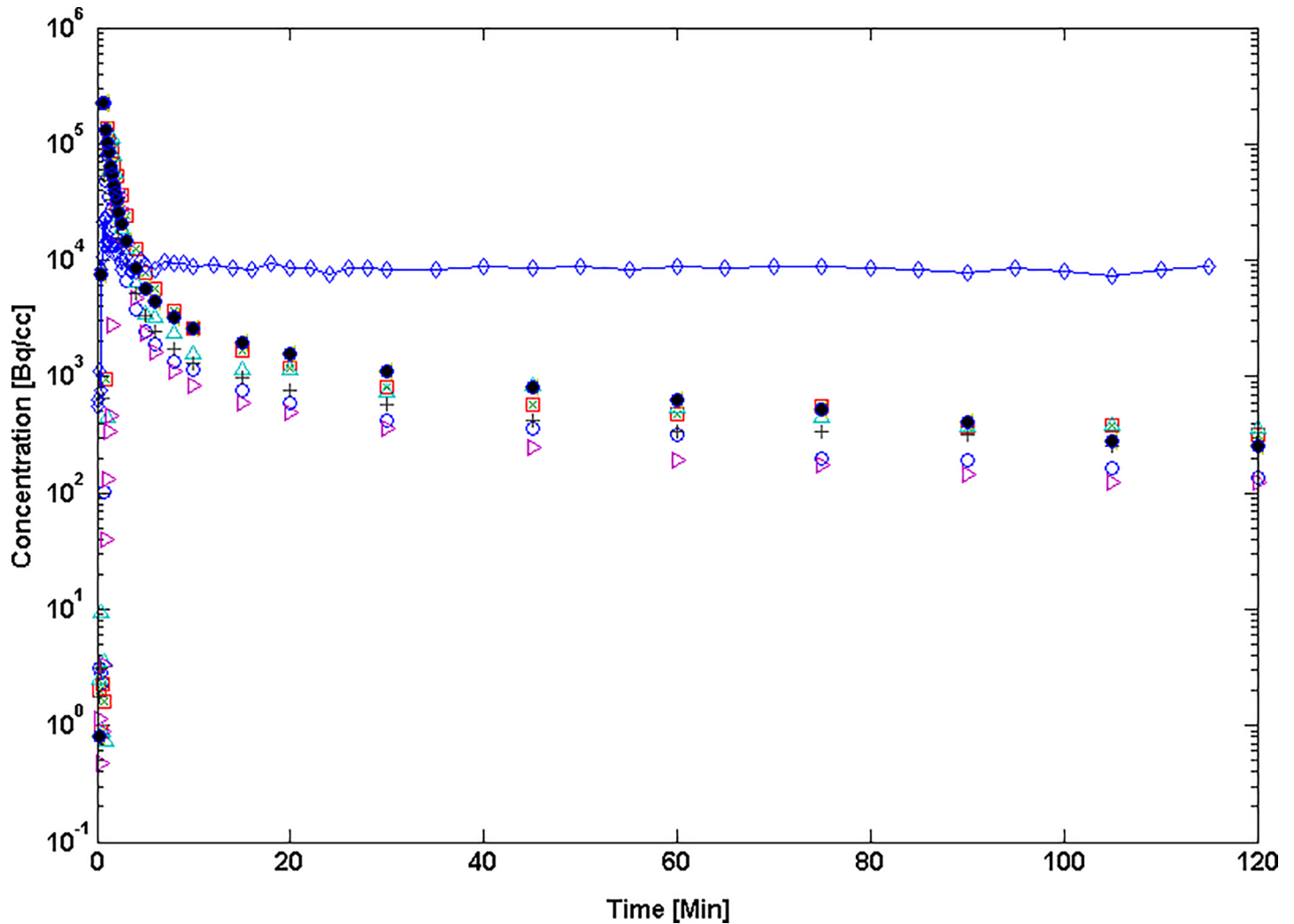


**Fig 3. Variation of plasma and tissue concentration following intravenous bolus injection of <sup>18</sup>F-TPP<sup>+</sup>.** Plasma concentration decreases monotonically over the first two hours; whereas, myocardial concentration is nearly constant.

<https://doi.org/10.1371/journal.pone.0190968.g003>

TPP<sup>+</sup> is avidly taken up by normal LV myocardium, as shown in Fig 5. The distribution of <sup>18</sup>F-TPP<sup>+</sup> is shown as SUV integrated from 60–120 min post tracer injection in the three oblique projections obtained directly from the PET image volume. No further processing was done to these images.

Representative parametric images of  $V_T$  and  $\Delta\Psi_T$  derived from kinetic data obtained from a control pig and an injury pig were reoriented into the standard cardiac coordinate system and presented in Fig 6. Images of  $V_T$  have units of cc-tissue/g-plasma; whereas, images of  $\Delta\Psi_T$  are in units of negative millivolts (-mV). The apparent lower volume of distribution in right ventricle and atria is artifactual, due to the thinner walls of those structures in combination with the effects of finite spatial resolution and cardiac motion blurring.

Segmental  $\Delta\Psi_T$  is tightly grouped for the five control pigs with a grand mean  $\pm$  SEM over 17 segments of  $-129.4 \pm 1.4$  mV (Fig 7). Values of  $\Delta\Psi_T$  are lower in injured segments, particularly in the apical-septal segments corresponding to the injury in the territory of the LAD artery.

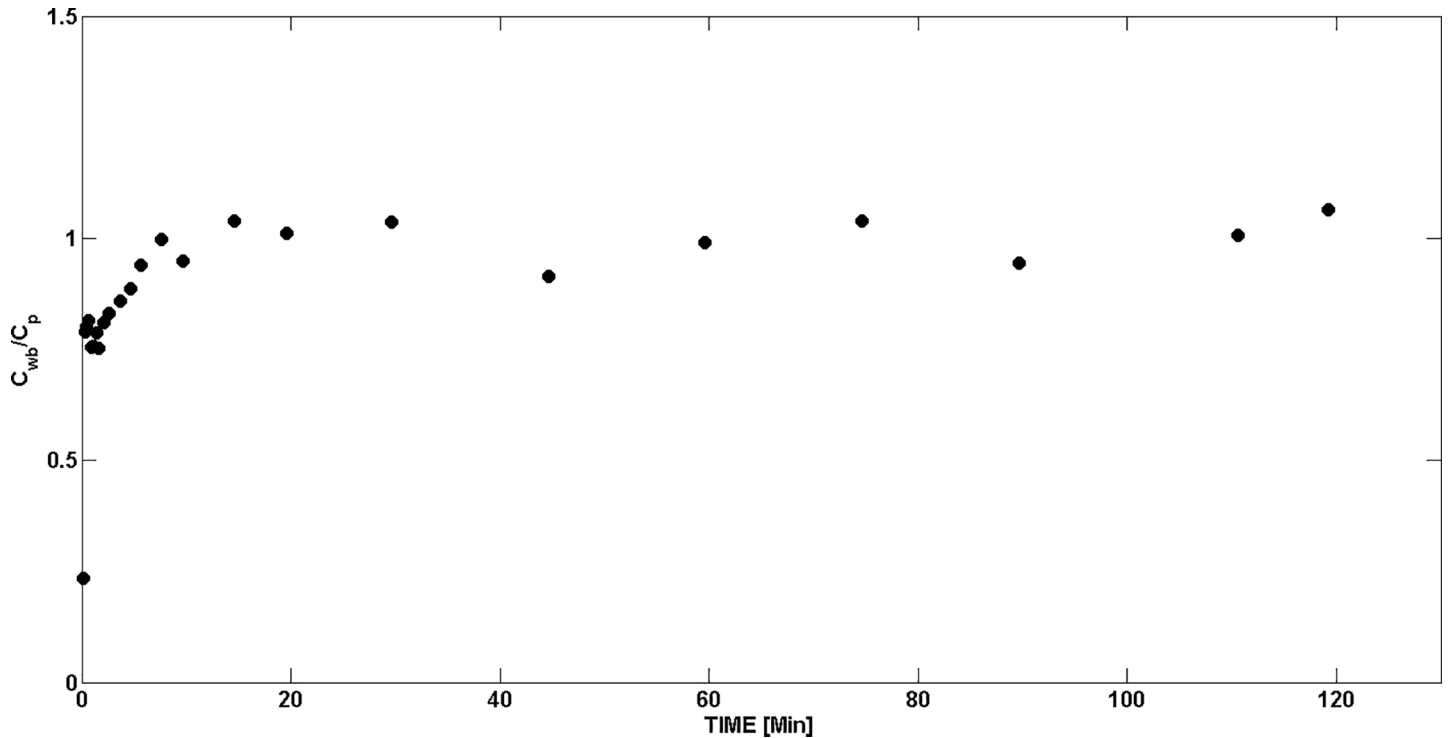


**Fig 4. Whole blood-to-plasma concentration ratio measured as a function of time after bolus injection of  $^{18}\text{F}$ -TPP $^+$ .** After about 15 minutes, whole blood and plasma concentrations equilibrate with equal concentration.

<https://doi.org/10.1371/journal.pone.0190968.g004>

## Discussion

In this paper, we introduce the concept of quantitative mapping of  $\Delta\Psi_T$  for monitoring mitochondrial status. Our development emphasizes measurement of the total membrane potential,  $\Delta\Psi_T$ , while making clear that  $\Delta\Psi_T$  is a proxy for and tightly correlated to  $\Delta\Psi_m$ . Direct measurements of  $\Delta\Psi_m$  require a separate measurement of the cellular membrane potential that is currently not possible in vivo. Just as in the early studies conducted with  $^3\text{H}$ -TPP $^+$ , our method relies on measuring the total concentration of a lipophilic cationic tracer which is then analyzed by using a compartment model of the tissue and the steady state formulation of the

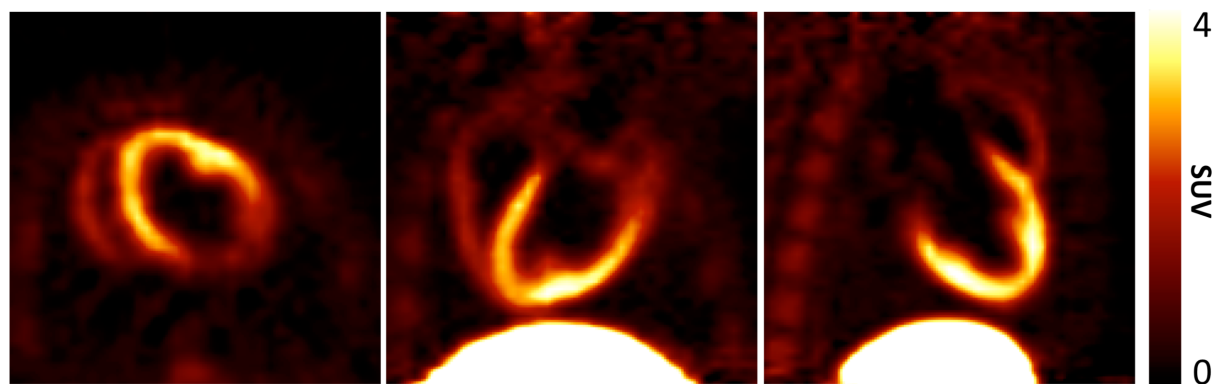


**Fig 5. Typical  $^{18}\text{F}$ -TPP $^+$  SUV image, integrated from 60–120 minutes after IV bolus injection.** SUV is highest in liver, followed by LV myocardium, with lower activity in the visible in bone marrow.

<https://doi.org/10.1371/journal.pone.0190968.g005>

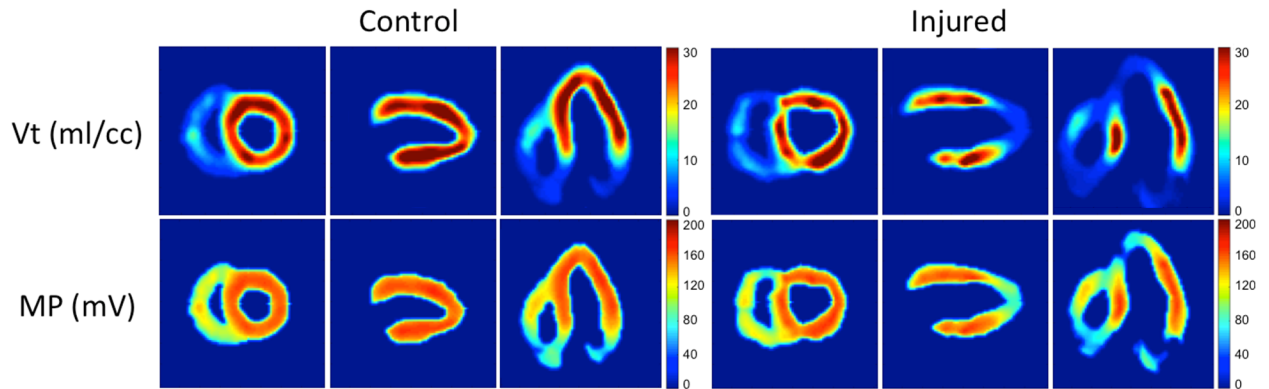


**Fig 6. Parametric images of  $V_T$  and  $\Delta\Psi_T$ .** Each panel of three x two images shows short axis, vertical and horizontal slices. Images of a representative control pig are shown in the left panel. Images of a representative scar pig are shown in the right panel. The top row of each panel depicts the TPP<sup>+</sup> volume of distribution and bottom row the membrane potential.

<https://doi.org/10.1371/journal.pone.0190968.g006>

Nernst equation, the same equation that is fundamental to electrochemistry [38] and cardiac electrophysiology [39, 40].

The relation of tracer concentration, which varies, and the physiological steady state can seem confusing. In the physiological state all the biological concentrations, transport rates and electropotentials are assumed to be fixed; whereas, the tracer concentrations evolve over time during the experiment (Fig 3). This complicates the application of the Nernst equation, whose use assumes the concentrations determining the membrane potential are invariant with time. We addressed that issue by using a kinetic model with extracellular and intracellular pools measured with dynamic PET to estimate the total volume of tracer distribution, a time invariant quantity characteristic of the tracer and the animal under study. We explicitly considered the effect of the electric field across the inner membrane of the mitochondrion on the kinetics

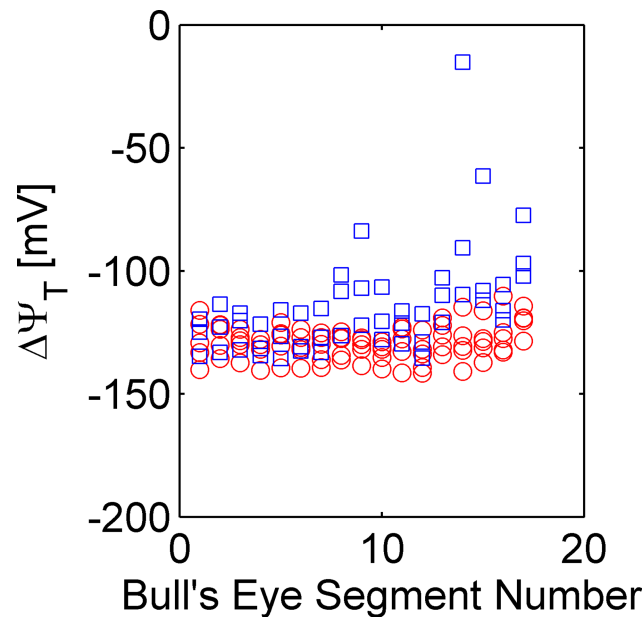


**Fig 7. Comparison of  $\Delta_T$  in 17 "bull's eye" segments Results shown for five control (blue squares) and three pigs with injury to the LAD territory (red circles).**

<https://doi.org/10.1371/journal.pone.0190968.g007>

of TPP<sup>+</sup> by using a kinetic model to express the relation between the total volume of distribution of the tracer and the electrical properties of the membrane. The structure of this model is identical to that used to analyze the classic <sup>3</sup>H-TPP<sup>+</sup> experiments conducted many years ago.

While qualitative imaging may serve many purposes, the quantitative aspects of our method may provide additional important information about mitochondrial status not available from visual inspection of images, true because mitochondrial dysfunction may, in some tissues, be associated with uniformly reduced  $\Delta\Psi_m$  and such conditions cannot be detected by qualitative imaging methods.

Another potentially important result of this work is the more analytic understanding of the factors affecting the distribution of TPP<sup>+</sup>, in particular, and voltage sensing tracers in general. We used basic principles of physics and physiology to show how the volume of distribution of lipophilic cations depends on the volume fractions of the tissue occupied by the ECS and the mitochondria as well as on the magnitude of  $\Delta\Psi_T$ .  $V_T$  is approximately equal to  $(1 - f_{ECS}) \cdot f_{mito} \cdot e^{-\Delta\Psi_T}$ . Keeping in mind that for normal tissue the mitochondrial membrane potential is about -140 mV [2] for all mitochondria regardless of tissue type; whereas, the fractional mitochondrial volume varies by more than a factor 10, Eqs 3 and 4 imply that the intensity of the  $V_T$  image will reflect the mitochondrial volume fraction of the tissue, thereby explaining the intensity variations depicted in Fig 5. Eqs 3 and 4 also make clear that the size of the ECS is an important factor when interpreting TPP<sup>+</sup> images because this quantity may vary with age and disease. Fig 2 shows the model-prediction for the volume of distribution when we fix the mitochondrial volume fraction while varying the membrane potential and the fractional volume of the ECS. This result shows that increases in the size of the ECS have decreasing effect on the total volume of distribution as the membrane potential decreases and becomes depolarized. But if the goal is to detect more subtle changes from normal  $\Delta\Psi_T$  it is important to include the effect of variation in ECS. Failure to account for changes in ECS may lead to unexplained variability in the qualitative and quantitative assessments of voltage-sensing tracer distribution.

$\Delta\Psi_m$  is sustained by the electron transport chain of the mitochondria, by which a balance is struck between protons pumped across the inner mitochondrial membrane and those pumped back to power the synthesis of ATP.  $\Delta\Psi_m$  is also affected by changes in the level of ROS and various mitochondrial ion channels [41]. Interestingly, increased ROS levels and modulation of mitochondrial ion channel function are seen early in numerous pathologies. Thus, the ability to quantitatively map  $\Delta\Psi_T$  may be useful for diagnosing or managing a number of such conditions. For example, reduction in  $\Delta\Psi_m$  has been implicated as a mechanism underlying ventricular arrhythmogenesis [42] and so might be used to improve the detection of arrhythmogenic foci.

We noted in Introduction that there are currently no methods for measuring  $\Delta\Psi_m$  in animal or human. This means that there is no independent method against which we can compare our PET methods. In this regard, it is important to emphasize that our noninvasive PET method is strongly related to the highly invasive and validated bench-top methods which preceded it. All prior methods employing in vitro application of cationic tracers were based on the Nernst equation to relate steady state concentrations and membrane potential in a compartment model of the mitochondrion, cell or tissue. Similarities to PET can be seen with <sup>3</sup>H-TPP<sup>+</sup> studies conducted in populations of cells and isolated mitochondria, where concentrations of TPP<sup>+</sup> in the medium are related to the concentration in ensembles of cells or mitochondria by the Nernst equation. Measurements with TPP<sup>+</sup> electrodes are also based on the same principles [9]. The similarity is most apparent in the work of Wan et al. [6] who studied  $\Delta\Psi_m$  in isolated rat hearts by using the arterio-venous difference in concentration of <sup>3</sup>H-TPP<sup>+</sup>

to infer the tissue-to-perfusate concentration ratio. *In essence, measuring the evolution of  $^{18}\text{F}\text{-TPP}^+$  concentration in a PET ROI is completely analogous to measurements with  $^3\text{H}\text{-TPP}^+$  in the isolated perfused rat heart studies of Wan et al. [6].* Hence, the PET studies are the natural extension of the classical bench top reference methods.

The fact that our PET measurements of  $\Delta\Psi_T$  are in accord with measurements in isolated rat hearts is an important observation, especially since direct validation of our method is impossible with existing methodologies. As illustrated in Table 1, the PET method yields results that are close to those found by the majority of prior studies, thereby providing additional support of our method.

With high specific activity, the mass of  $^{18}\text{F}\text{-TPP}^+$  is  $10^{-10}$  to  $10^{-7}$  lower than the intracellular potassium concentration, meaning its effect on membrane potential is negligible. However, it is worth mentioning that prior studies with  $^3\text{H}\text{-TPP}^+$  have sometimes made corrections for non-specific binding of  $\text{TPP}^+$  [4] but the literature is not concordant on the necessity of correction [4, 9, 43–45]. Furthermore, previous bench top studies used very low specific activity  $\text{TPP}^+$ , complicating an evaluation of its necessity in tracer measurements. Nevertheless, similar corrections could be applied to the PET analyses, but were found to be unnecessary to establish initial validity.

Close inspection of Fig 5 shows there is a high value of  $V_T$  in normal myocardium, with mitochondrial concentrations nearly 30 times the plasma level. At secular equilibrium, the inward and outward fluxes across the mitochondrial membrane have to balance, meaning that outward clearance must be about 30 times lower than the inward rate, thereby explaining the slow clearance observed experimentally after bolus injection of  $^{18}\text{F}\text{-TPP}^+$ . Fig 5 also shows that the volume of distribution in injured myocardium is much lower, with tissue concentrations less than 10 times the plasma concentration. Our kinetic model shows that  $V_T$  depends linearly on  $f_{ECS}$  and exponentially on  $\Delta\Psi_T$ . Accordingly, we have converted  $V_T$  to an estimate of  $\Delta\Psi_T$  by accounting for the effects of  $f_{ECS}$ , a quantity known to vary in age and disease [46–49]. Thus, we have shown it will be necessary to account for changes in extracellular volume fraction in clinical studies to obtain the full benefit of such studies.

A marked difference in contrast between  $V_T$  and  $\Delta\Psi_T$  was observed between normal and injured tissue (Fig 5). Both  $V_T$  and  $\Delta\Psi_T$  are quantitative measures emphasizing different aspects of  $^{18}\text{F}\text{-TPP}^+$  distribution. On one hand,  $V_T$  is the total volume of  $^{18}\text{F}\text{-TPP}^+$  distribution, including effects due to  $\Delta\Psi_T$ ,  $f_{ECS}$ , and  $f_{mito}$ . Therefore, mitochondrial density ( $f_{mito}$ ) will affect the relative uptake of a voltage-sensing tracer. This finding is interesting given that different pathologies are associated with reduced mitochondrial density. For example, a reduction in mitochondrial density is seen in the skeletal muscles of patients with chronic obstructive pulmonary disease [50]. In these conditions,  $V_T$  measurements would provide an overall quantitative measure of mitochondrial status in tissue. On the other hand,  $\Delta\Psi_T$  focuses predominantly on the electrochemical conditions that prevail at the inner mitochondrial membrane. In the large tissue injury, we see that there is an area of profound reduction in  $\Delta\Psi_T$ , approaching total depolarization. Other parts of the injured region show lesser depolarization in the range of -60 mV, but still very different than  $\Delta\Psi_T$  in normal myocardium. This can also be appreciated from the data in Fig 7, where the blue circles indicate major reductions in the average  $\Delta\Psi_T$  for bull's eye segment 8, 9, 14, 15 and 17. We can also see the variability of tissue injury expressed in Fig 7, which demonstrate a patchy nature to those injuries that might be better appreciated by direct examination of the parametric images.

As also shown in Fig 7, pigs in the control group exhibited segmental values of  $\Delta\Psi_T$  that averaged about  $-129.4 \pm 1.4$  mV (SEM). The tight grouping of  $\Delta\Psi_T$  measurements over all normal segments and pigs is remarkable. The kinetic approach, used in this study, requires a long measurement period for accurate estimation of the total volume of distribution. A protocol

using primed constant infusion may be preferred for human investigation in order to restrict actual scan time to the equilibrium period, 95–120 min.

In this work we reported the results of kinetic analysis using the Logan graphical method, which is known to underestimate  $V_T$  with increasing statistical noise in the measurements[51]. We mitigated the effect of statistical noise by averaging  $\Delta\Psi_T$  maps for 17 polar segments but the reader should be aware that the spatial averaging also causes some underestimation of  $\Delta\Psi_T$ . We also formed parametric images using the reGP method of Zhou et al [52] and the total least squares approach of Varga and Szabo,[53] but these methods yielded noisy parametric images; overall, they were not an improvement over the Logan plot.

## Conclusions

This study is the first to demonstrate the feasibility of quantitative in vivo mapping of total membrane potential,  $\Delta\Psi_T$ , a proxy of  $\Delta\Psi_m$ . In vivo measurements of  $\Delta\Psi_T$  obtained with our new method yielded values remarkably constant within and across the hearts of domestic swine that are comparable to results from in vitro bench top experiments. We have derived a theory explaining, for the first time, the major factors affecting the transport and residence time of lipophilic cations in tissue, including  $\Delta\Psi_T$  and  $f_{ECS}$ . The fact that we can measure  $\Delta\Psi_T$  in mV suggests that it may be possible to compare individual's studies with normative data. Given the critical role of mitochondrial function in numerous pathologies, the potential applications of this new imaging method are immense. This novel technique could eventually be proved useful in numerous clinical and research scenarios.

## Acknowledgments

The authors thank Kevin Cordaro, Victoria Douglas and Julia Scotton for animal preparation, handling and monitoring. We are also grateful to Dr. Moses Wilks and Dr. Eline Verwer for their help during experimental measurements. We also thank Henry Gewirtz, M.D. for helpful discussions.

## Author Contributions

**Conceptualization:** Nathaniel M. Alpert, Moussa C. Mansour, Yun Zhou, Timothy M. Shoup.

**Data curation:** Nicolas Guehl.

**Formal analysis:** Nathaniel M. Alpert, Nicolas Guehl.

**Funding acquisition:** Georges El Fakhri.

**Investigation:** Nathaniel M. Alpert, Leon Ptaszek, Matthieu Pelletier-Galarneau, Dustin Wooten, Chao Ma, Kazue Takahashi, Georges El Fakhri.

**Methodology:** Nathaniel M. Alpert, Nicolas Guehl, Leon Ptaszek, Jeremy Ruskin, Moussa C. Mansour, Dustin Wooten, Chao Ma, Kazue Takahashi, Yun Zhou, Timothy M. Shoup, Marc D. Normandin, Georges El Fakhri.

**Project administration:** Georges El Fakhri.

**Resources:** Jeremy Ruskin, Moussa C. Mansour.

**Writing – original draft:** Nathaniel M. Alpert.

**Writing – review & editing:** Nathaniel M. Alpert, Nicolas Guehl, Leon Ptaszek, Matthieu Pelletier-Galarneau, Yun Zhou, Marc D. Normandin, Georges El Fakhri.

## References

1. Rich P. Chemiosmotic coupling: the cost of living. *Nature*. 2003; 421(6923):583–. <https://doi.org/10.1038/421583a> PMID: 12571574
2. Alberts B, Johnson A, Lewis J, Walter P, Raff M, Roberts K. *Molecular Biology of the Cell 4th Edition: International Student Edition*. Routledge; 2002.
3. Kauppinen RA HI. Monitoring of mitochondrial membrane potential in isolated perfused rat heart. *Am J Physiol*. 1984; 247(508–516).
4. Rottenberg H. Membrane potential and surface potential in mitochondria: uptake and binding of lipophilic cations. *The Journal of membrane biology*. 1984; 81(2):127–38. PMID: 6492133
5. LaNoue KF, Strzelecki T, Strzelecka D, Koch C. Regulation of the uncoupling protein in brown adipose tissue. *Journal of Biological Chemistry*. 1986; 261(1):298–305. PMID: 3941078
6. Wan B, Doumen C, Duszynski J, Salama G, Vary TC, LaNoue KF. Effects of cardiac work on electrical potential gradient across mitochondrial membrane in perfused rat hearts. *American Journal of Physiology*. 1993; 265:H453–H. <https://doi.org/10.1152/ajpheart.1993.265.2.H453> PMID: 8368348
7. Gurm GS, Danik SB, Shoup TM, Weise S, Takahashi K, Laferrier S, et al. 4-[<sup>18</sup>F]-tetraphenylphosphonium as a PET tracer for myocardial mitochondrial membrane potential. *JACC Cardiovascular imaging*. 2012; 5(3):285–92. <https://doi.org/10.1016/j.jcmg.2011.11.017> PMID: 22421174
8. Gerencser AA, Chinopoulos C, Birket MJ, Jastroch M, Vitelli C, Nicholls DG, et al. Quantitative measurement of mitochondrial membrane potential in cultured cells: calcium-induced and hyperpolarization of neuronal mitochondria. *The Journal of physiology*. 2012; 590(12):2845–71. <https://doi.org/10.1113/jphysiol.2012.228387> PMID: 22495585
9. Kamo N, Muratsugu M, Hongoh R, Kobatake Y. Membrane potential of mitochondria measured with an electrode sensitive to tetraphenyl phosphonium and relationship between proton electrochemical potential and phosphorylation potential in steady state. *The Journal of membrane biology*. 1979; 49(2):105–21. PMID: 490631
10. Huttemann M, Lee I, Pecinova A, Pecina P, Przyklenk K, Doan JW. Regulation of oxidative phosphorylation, the mitochondrial membrane potential, and their role in human disease. *Journal of bioenergetics and biomembranes*. 2008; 40(5):445–56. <https://doi.org/10.1007/s10863-008-9169-3> PMID: 18843528
11. Pfeffer G, Chinnery PF. Diagnosis and treatment of mitochondrial myopathies. *Annals of medicine*. 2013; 45(1):4–16. <https://doi.org/10.3109/07853890.2011.605389> PMID: 21867371
12. De Felice FG, Ferreira ST. Inflammation, defective insulin signaling, and mitochondrial dysfunction as common molecular denominators connecting type 2 diabetes to Alzheimer disease. *Diabetes*. 2014; 63(7):2262–72. <https://doi.org/10.2337/db13-1954> PMID: 24931033
13. Pohanka M. Alzheimer's disease and oxidative stress: a review. *Current medicinal chemistry*. 2014; 21(3):356–64. PMID: 24059239
14. O'Rourke B. Metabolism: Beyond the power of mitochondria. *Nature Reviews Cardiology*. 2016; 13(7):386–8. <https://doi.org/10.1038/nrcardio.2016.95> PMID: 27303815
15. Summerhayes IC, Lampidis TJ, Bernal SD, Nadakavukaren JJ, Nadakavukaren KK, Shepherd EL, et al. Unusual retention of rhodamine 123 by mitochondria in muscle and carcinoma cells. *Proc Natl Acad Sci U S A*. 1982; 79(17):5292–6. PMID: 6752944
16. Nunnari J, Suomalainen A. Mitochondria: in sickness and in health. *Cell*. 2012; 148(6):1145–59. <https://doi.org/10.1016/j.cell.2012.02.035> PMID: 22424226
17. Rutledge C, Dudley S. Mitochondria and arrhythmias. *Expert Rev Cardiovasc Ther*. 2013; 11(7):799–801. <https://doi.org/10.1586/14779072.2013.811969> PMID: 23895021
18. Chen LB. Mitochondrial membrane potential in living cells. *Annual review of cell biology*. 1988; 4(1):155–81.
19. Johnson LV, Walsh ML, Bockus BJ, Chen LB. Monitoring of relative mitochondrial membrane potential in living cells by fluorescence microscopy. *The Journal of Cell Biology*. 1981; 88(3):526–35. PMID: 6783667
20. Moreno AnJ Santos DL, Magalhaes Novais S Oliveira PJ. Measuring Mitochondrial Membrane Potential with a Tetraphenylphosphonium Selective Electrode. *Current Protocols in Toxicology*. 2015;25.5. 1–5. 16.
21. J Ritchie R. A critical assessment of the use of lipophilic cations as membrane potential probes. *Progress in biophysics and molecular biology*. 1984; 43(1):1–32. PMID: 6374760
22. Kauppinen R. Proton electrochemical potential of the inner mitochondrial membrane in isolated perfused rat hearts, as measured by exogenous probes. *Biochimica et Biophysica Acta (BBA)-Bioenergetics*. 1983; 725(1):131–7.

23. Lichtshtein D, Kaback HR, Blume AJ. Use of a lipophilic cation for determination of membrane potential in neuroblastoma-glioma hybrid cell suspensions. *Proceedings of the National Academy of Sciences of the United States of America*. 1979; 76(2):650–4. PMID: [284390](#)
24. Logan A, Pell VR, Shaffer KJ, Evans C, Stanley NJ, Robb EL, et al. Assessing the mitochondrial membrane potential in cells and in vivo using targeted click chemistry and mass spectrometry. *Cell metabolism*. 2016; 23(2):379–85. <https://doi.org/10.1016/j.cmet.2015.11.014> PMID: [26712463](#)
25. Min J-J, Biswal S, Deroose C, Gambhir SS. Tetraphenylphosphonium as a novel molecular probe for imaging tumors. *Journal of Nuclear Medicine*. 2004; 45(4):636–43. PMID: [15073261](#)
26. Shoup TM, Elmaleh DR, Brownell AL, Zhu A, Guerrero JL, Fischman AJ. Evaluation of (4-[<sup>18</sup>F]Fluorophenyl)triphenylphosphonium ion. A potential myocardial blood flow agent for PET. *Mol Imaging Biol*. 2011; 13(3):511–7. <https://doi.org/10.1007/s11307-010-0349-2> PMID: [20563755](#)
27. Kawamoto A, Kato T, Shioi T, Okuda J, Kawashima T, Tamaki Y, et al. Measurement of technetium-99m sestamibi signals in rats administered a mitochondrial uncoupler and in a rat model of heart failure. *PLoS one*. 2015; 10(1):e0117091. <https://doi.org/10.1371/journal.pone.0117091> PMID: [25594546](#)
28. Kim D-Y, Kim H-S, Le UN, Jiang SN, Kim H-J, Lee K-C, et al. Evaluation of a mitochondrial voltage sensor, (18F-fluoropentyl) triphenylphosphonium cation, in a rat myocardial infarction model. *Journal of Nuclear Medicine*. 2012; 53(11):1779–85. <https://doi.org/10.2967/jnumed.111.102657> PMID: [23038748](#)
29. Madar I, Huang Y, Ravert H, Dalrymple SL, Davidson NE, Isaacs JT, et al. Detection and quantification of the evolution dynamics of apoptosis using the PET voltage sensor 18F-fluorobenzyl triphenyl phosphonium. *Journal of Nuclear Medicine*. 2009; 50(5):774–80. <https://doi.org/10.2967/jnumed.108.061283> PMID: [19372481](#)
30. Madar I, Ravert H, Nelkin B, Abro M, Pomper M, Dannals R, et al. Characterization of membrane potential-dependent uptake of the novel PET tracer 18F-fluorobenzyl triphenylphosphonium cation. *Eur J Nucl Med Mol Imaging*. 2007; 34(12):2057–65. <https://doi.org/10.1007/s00259-007-0500-8> PMID: [17786439](#)
31. Kim D-Y, Kim HS, Reder S, Zheng JH, Herz M, Higuchi T, et al. Comparison of 18F-Labeled Fluoroalkylphosphonium Cations with <sup>13</sup>N-NH<sub>3</sub> for PET Myocardial Perfusion Imaging. *Journal of Nuclear Medicine*. 2015; 56(10):1581–6. <https://doi.org/10.2967/jnumed.115.156794> PMID: [26069304](#)
32. Nernst W. Die elektromotorische wirksamkeit der jonen. *Zeitschrift für physikalische Chemie*. 1889; 4(1):129–81.
33. Nernst W. *Experimental and theoretical applications of thermodynamics to chemistry*: C. Scribner's sons; 1907.
34. Barth E, Stämmler G, Speiser B, Schaper J. Ultrastructural quantitation of mitochondria and myofilaments in cardiac muscle from 10 different animal species including man. *Journal of molecular and cellular cardiology*. 1992; 24(7):669–81. PMID: [1404407](#)
35. Seldinger SI. Catheter replacement of the needle in percutaneous arteriography: a new technique. *Acta radiologica*. 1953; 39(5):368–76. PMID: [13057644](#)
36. Bandula S, White SK, Flett AS, Lawrence D, Pugliese F, Ashworth MT, et al. Measurement of myocardial extracellular volume fraction by using equilibrium contrast-enhanced CT: validation against histologic findings. *Radiology*. 2013; 269(2):396–403. <https://doi.org/10.1148/radiol.13130130> PMID: [23878282](#)
37. Logan J, Fowler JS, Volkow ND, Wolf AP, Dewey SL, Schlyer DJ, et al. Graphical analysis of reversible radioligand binding from time-activity measurements applied to [<sup>11</sup>C-methyl]-(<sup>11</sup>C)-cocaine PET studies in human subjects. *Journal of Cerebral Blood Flow & Metabolism*. 1990; 10(5):740–7.
38. Bockris JOM, Reddy AK. *Modern electrochemistry: an introduction to an interdisciplinary area*: Springer Science & Business Media; 2012.
39. Whalley DW, Wendt DJ, Grant AO. Basic concepts in cellular cardiac electrophysiology: Part I: Ion channels, membrane currents, and the action potential. *Pacing and Clinical Electrophysiology*. 1995; 18(8):1556–74. PMID: [7479177](#)
40. Iwai S, Markowitz SM, Lerman BB. *Electrophysiology of Cardiac Arrhythmias*. Essential Cardiology: Springer; 2013. p. 261–75.
41. O'Rourke B, Cortassa S, Aon MA. Mitochondrial ion channels: gatekeepers of life and death. *Physiology*. 2005; 20(5):303–15.
42. Brown DA, O'rourke B. Cardiac mitochondria and arrhythmias. *Cardiovascular research*. 2010; 88(2):241–9. <https://doi.org/10.1093/cvr/cvq231> PMID: [20621924](#)
43. Aiuchi T, Matsunaga M, Nakaya K, Nakamura Y. Calculation of membrane potential in synaptosomes with use of a lipophilic cation (tetraphenylphosphonium). *Chemical and Pharmaceutical Bulletin*. 1989; 37(12):3333–7. PMID: [2632080](#)

44. Demura M, Kamo N, Kobatake Y. Mitochondrial membrane potential estimated with the correction of probe binding. *Biochimica et Biophysica Acta (BBA)-Bioenergetics*. 1987; 894(3):355–64.
45. Labajova A, Vojtiskova A, Krivakova P, Kofranek J, Drahota Z, Houstek J. Evaluation of mitochondrial membrane potential using a computerized device with a tetraphenylphosphonium-selective electrode. *Analytical biochemistry*. 2006; 353(1):37–42. <https://doi.org/10.1016/j.ab.2006.03.032> PMID: 16643832
46. Wong TC, Piehler KM, Kang IA, Kadakkal A, Kellman P, Schwartzman DS, et al. Myocardial extracellular volume fraction quantified by cardiovascular magnetic resonance is increased in diabetes and associated with mortality and incident heart failure admission. *European heart journal*. 2012; eht193.
47. Ho CY, Abbasi SA, Neilan TG, Shah RV, Chen Y, Heydari B, et al. T1 measurements identify extracellular volume expansion in hypertrophic cardiomyopathy sarcomere mutation carriers with and without left ventricular hypertrophy. *Circulation: Cardiovascular Imaging*. 2012; 6(3):415–22.
48. Sado DM, Flett AS, Banypersad SM, White SK, Maestrini V, Quarta G, et al. Cardiovascular magnetic resonance measurement of myocardial extracellular volume in health and disease. *Heart*. 2012; heartjnl-2012-302346.
49. Schelbert EB, Testa SM, Meier CG, Ceyrolles WJ, Levenson JE, Blair AJ, et al. Myocardial extravascular extracellular volume fraction measurement by gadolinium cardiovascular magnetic resonance in humans: slow infusion versus bolus. *Journal of Cardiovascular Magnetic Resonance*. 13(1):16.
50. Liu S-F, Kuo H-C, Tseng C-W, Huang H-T, Chen Y-C, Tseng C-C, et al. Leukocyte mitochondrial DNA copy number is associated with chronic obstructive pulmonary disease. *PloS one*. 2015; 10(9): e0138716. <https://doi.org/10.1371/journal.pone.0138716> PMID: 26394041
51. Slifstein M, Laruelle M. Effects of statistical noise on graphic analysis of PET neuroreceptor studies. *Journal of Nuclear Medicine*. 2000; 41(12):2083–8. PMID: 11138696
52. Zhou Y, Ye W, Brasic JR, Crabb AH, Hilton J, Wong DF. A consistent and efficient graphical analysis method to improve the quantification of reversible tracer binding in radioligand receptor dynamic PET studies. *Neuroimage*. 2009; 44(3):661–70. <https://doi.org/10.1016/j.neuroimage.2008.09.021> PMID: 18930830
53. Jz Varga, Szabo Z. Modified regression model for the Logan plot. *Journal of Cerebral Blood Flow & Metabolism*. 2002; 22(2):240–4.